Lattice vibration fundamentals in nanocrystalline anatase investigated with Raman scattering

2008 J. Phys.: Condens. Matter 20 085212

(http://iopscience.iop.org/0953-8984/20/8/085212)

IOP PUBLISHING JOURNAL OF PHYSICS: CONDENSED MATTER

J. Phys.: Condens. Matter **20** (2008) 085212 (7pp) doi:10.1088/0953-8984/20/8/085212

Lattice vibration fundamentals in nanocrystalline anatase investigated with Raman scattering

D Wang[1], J Zhao[1], B Chen[1] and C Zhu[2]

[1] Hefei National Laboratory for Physical Sciences at Microscale, University of Science and Technology of China, Hefei, Anhui 230026, People's Republic of China
[2] Department of Material Science and Engineering, University of Science and Technology of China, Hefei, Anhui 230026, People's Republic of China

E-mail: eedewang@ustc.edu.cn

Received 28 November 2007
Published 1 February 2008
Online at stacks.iop.org/JPhysCM/20/085212

Abstract

A detailed nano-size and temperature-dependent Raman scattering study of the $E_{g(1)}$ mode was carried out from 83 to 723 K for nanocrystalline anatase with sizes of 5.6, 8.6, and 19.4 nm. The $E_{g(1)}$ Raman spectra were fitted and calculated on the basis of a combined model of both anharmonic coupling and phonon confinement. The temperature-dependent lattice vibration fundamentals are essentially the same for all these three nanocrystallites. Both the three- and four-phonon processes are needed to obtain excellent fitting, and the main contribution comes from the three-phonon processes. The anharmonic-decay-related phonon lifetime increases with decreasing nanocrystallite size, and the smaller nanoparticles have slower anharmonic decay. The phonon confinement has a comparative effect on both the linewidth broadening and the peak frequency shift, and it is responsible for a much shorter phonon lifetime at low temperatures for the 5.6 nm nanocrystallite.

1. Introduction

The lattice vibration in a nanocrystallite may present new aspects in the vibration fundamentals due to the nano-size effect [1–8]. In an isolated nanoparticle, a plane-wave-like phonon wavefunction cannot exist within the particle because of the existence of the crystal surface. The lattice vibration waves get reflected and/or decay at the boundary. They remain confined within the particle (phonon confinement effect). To describe this confinement effect, the plane-wave-like wavefunction is multiplied by a Gaussian confinement function, which decays to a very small value at the nanoparticle free surface [1, 3, 5–7]. The spatial restriction on the phonon wavefunction is noticeable only when the particle size, d, is smaller than ~20 lattice parameters. This restriction results in a relaxation of the $q \approx 0$ selection rule for the first-order Raman scattering process. All the lattice vibration modes with wavevectors in a range of $\Delta q \sim \pi/d$ around the Brillouin zone center can participate in the Raman scattering process. Depending on the negative or positive dispersion curves, whose phonon frequencies decrease or increase as a function of wavenumber, the Raman spectra usually develop marked asymmetry towards the low- or high-frequency sides, respectively.

Titanium dioxide TiO_2 material is one of the most investigated transition-metal oxide materials due to its wide application possibilities. TiO_2 can be used in the fields of optical filters, optical waveguides, chemical sensors, solar cells, and more [9–11]. The lattice vibration fundamentals and optical properties of single-crystal and nanocrystalline TiO_2 have been studied by both experimental and theoretical methods [12–19]. The lattice vibration properties of these two types of crystals should, on the one hand, have similar properties, which are determined by the fundamental crystal structure, and on the other hand the nanocrystalline anatase should have its own characteristics, such as the phonon confinement effect as discussed above. It was reported that the frequency variations of the $E_{g(1)}$ and $E_{g(3)}$ modes with temperature are more linear in single crystals than in nanocrystals [18]. Phonon coupling is enhanced in anatase TiO_2 nanocrystal [2]. The temperature dependences of both the Raman shifts and Raman peak linewidths were reported to

behave differently in single-crystal and nanocrystalline TiO_2. For the $E_{g(1)}$ mode, in nanocrystalline TiO_2, only three-phonon processes were considered to contribute to both the frequency hardening and linewidths, while in single-crystal TiO_2 the Raman shift arose from strong four-phonon processes and the linewidth came from three-phonon processes [2, 20]. Whether the phonon coupling is enhanced or not in a nanodimensional crystallite, the reported results are not consisted with each other [2, 5]. In order to clarify these conflicting fine differences between nano-crystallites and bulk crystals, a detailed and careful experimental setup as well as good theoretical fittings need to be carried out.

In this paper, a detailed nano-size and temperature-dependent micro-Raman scattering study was carried out for nanocrystalline anatase with different grain sizes. In order to analyze the Raman spectra evolution with sizes and temperatures, the possible contributory factors, such as phonon confinement, thermal expansion, anharmonic phonon coupling, grain size distribution, and surface stress, were considered. A rather reasonable image concerning the nanocrystalline vibrational fundamentals is given in this paper, and this clears up some inconsistencies that are found in publications.

2. Experiments

Anatase nanocrystalline TiO_2 powders were prepared by the sol–gel process. Titanium butoxide ($Ti(OC_4H_9)_4$), acetic acid, deionized water (with a resistivity of 18 MΩ), and absolute ethanol were used as the reaction precursors. Polyethyleneglycol 400 was added into the formed sols as the complexing agent. The gels that were prepared could be stable for up to several months, which allowed us to obtain reproducible TiO_2 powders with very homogeneous particle size distributions. The gels were heated in an autoclave for several hours at different temperatures from 120 to 450 °C. The TiO_2 colloids were dried at 100 °C. Then the ground powders were washed with ethanol by centrifuge. X-ray diffraction data showed only the anatase peaks; no rutile peaks were observed after the heat treatment at 450 °C. A strong (101) peak indicated that the anatase powders preferably crystallized with (101) facets. The full width at half maximum (FWHM) of the (101) peak was used to calculate the nanoparticle size, which is given by the Scherrer formula. TiO_2 powders with three nano-sizes, namely 5.6, 8.6, and 19.4 nm, were prepared on the basis of the following two reasons. When the nanocrystallite size is smaller than ∼3–4 nm, the phonon dispersion curve and the shape of the Brillouin zone may be much different from that of bulk TiO_2 crystal [21]. For a nanoparticle larger than ∼20 nm, its lattice dynamic characteristics, such as the phonon frequencies, approach that of bulk TiO_2 crystal [22]. Therefore, the 19.4 nm TiO_2 nanocrystallite can act as a bulk-like TiO_2 reference. The Raman spectra were taken by using a LABRAM-HR micro-Raman system with a laser wavelength of 514 nm. The laser light diameter is ∼7 μm. Temperature-dependent Raman spectroscopy was carried out between 83 and 723 K at an increasing rate of ∼4 K min^{-1}. When an experimental temperature was reached, the temperature was kept stable for up to 2 min before a Raman spectrum was taken. A nonlinear curve fitting program in OriginPro 7.0 was used to perform the fittings for the peak frequency and the linewidth. After the subtraction of a baseline from the Raman spectrum, a pure Lorentzian function was used to fit the peak curve to obtain the peak values and linewidths. MatLab 6.5 was used for the Raman spectra calculations.

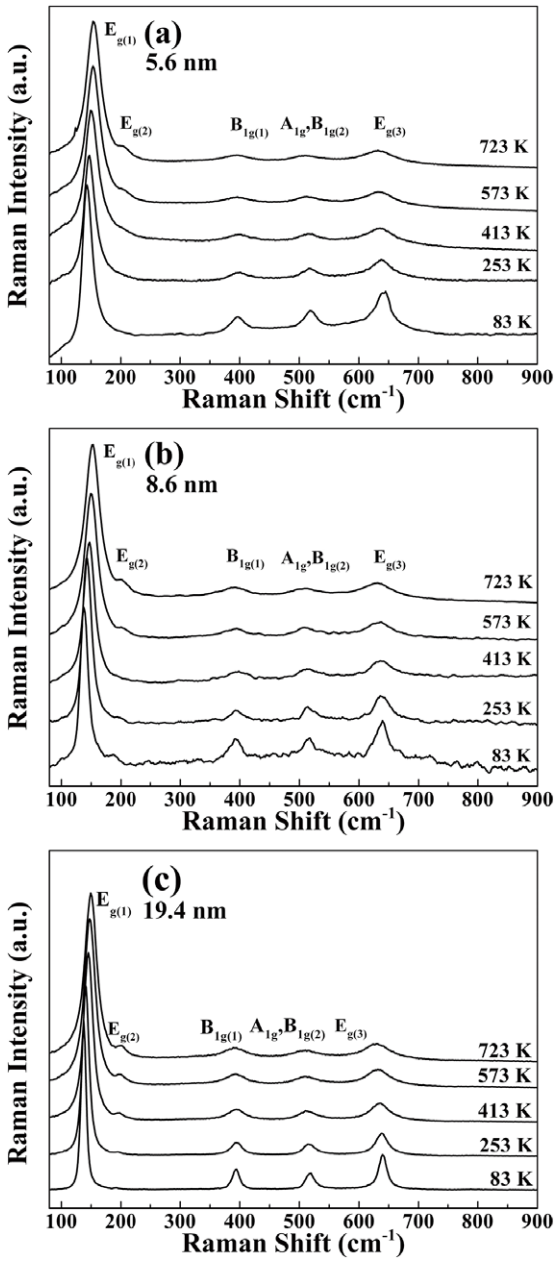

Figure 1. $E_{g(1)}$ Raman spectra recorded at different temperatures for (a) 5.6 nm, (b) 8.6 nm, and (c) 19.4 nm nanocrystallites.

3. Experimental results and discussions

Figure 1 shows Raman spectra recorded at different temperatures for 5.6, 8.6, and 19.4 nm nanocrystalline TiO_2, respectively. All six Raman active modes, $3E_g + 2B_{1g} + A_{1g}$, were observed. The observation of the $E_{g(2)}$ mode, which is

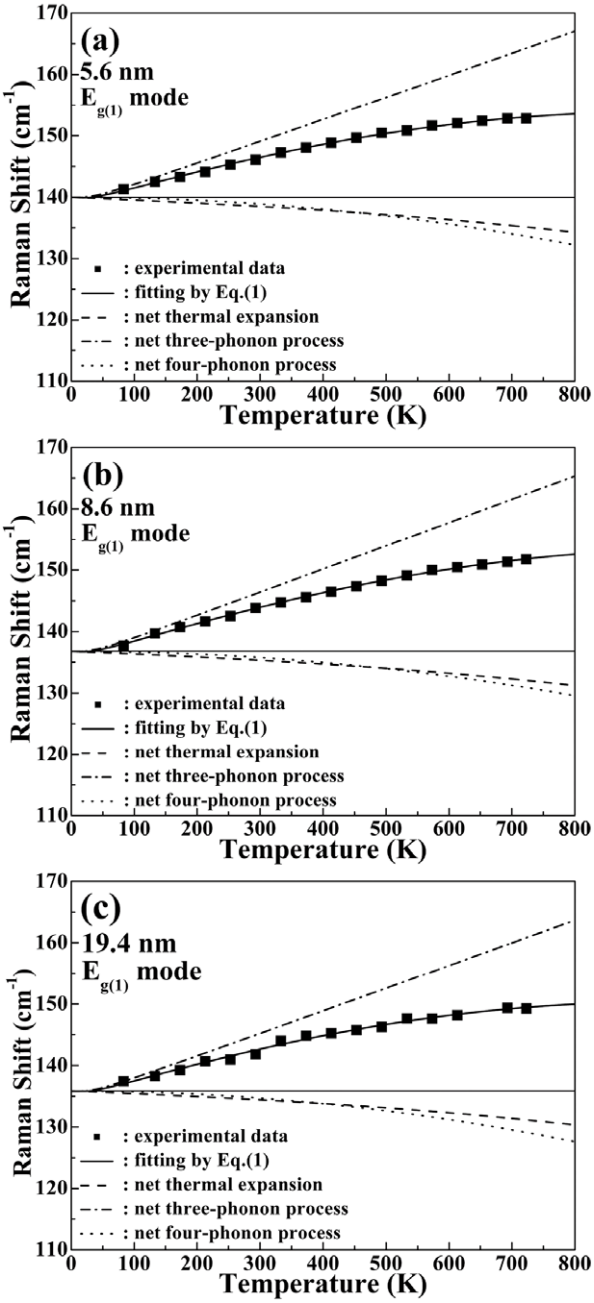

Figure 2. Experimental and three-parameter fittings of temperature dependences of $E_{g(1)}$ frequencies for (a) 5.6 nm, (b) 8.6 nm, and (c) 19.4 nm nanocrystallites. The fitting lines show contributions from the thermal expansion, three-phonon, and four-phonon processes, respectively.

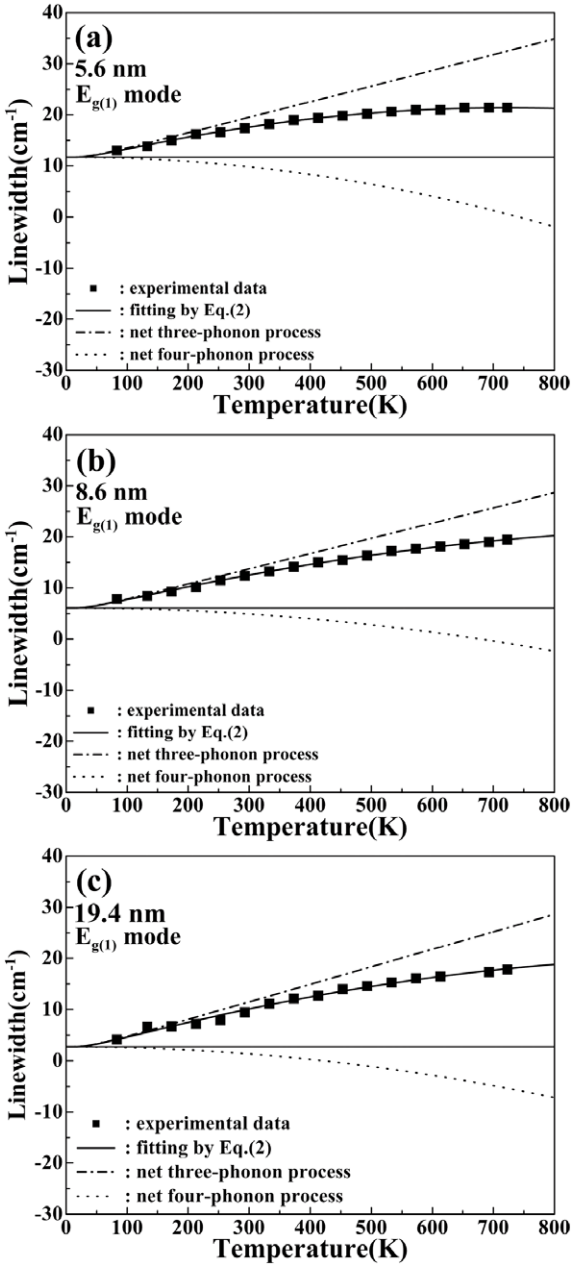

Figure 3. Experimental and three-parameter fittings of temperature dependences of $E_{g(1)}$ linewidth of (a) 5.6 nm, (b) 8.6 nm, and (c) 19.4 nm nanocrystallites. The fitting lines show contributions from three-phonon and four-phonon processes, respectively.

usually hard to detect, is evidence of a well-ordered crystalline structure even for the 5.6 nm anatase nanoparticles. In this report, in order to compare the experimental data precisely with that of theoretical calculations, we use the strongest peak, namely the $E_{g(1)}$ peak, for the detailed analyses.

The temperature-dependent $E_{g(1)}$ frequency shift and linewidths are shown in figures 2 and 3. It is widely accepted that two effects contribute to the Raman shift with temperature: the thermal expansion and the anharmonic coupling to phonons of other branches [5, 23–26]. The temperature-dependent Raman shift can be written as [23]:

$$\omega(T) = (\omega(0) - p_1 - p_2)\exp\left[-\gamma\int_0^T (2\alpha_\perp(T') + \alpha_\parallel(T'))\,\mathrm{d}T'\right] + p_1\left(1 + \frac{2}{\mathrm{e}^x - 1}\right) + p_2\left(1 + \frac{3}{\mathrm{e}^y - 1} + \frac{3}{(\mathrm{e}^y - 1)^2}\right) \quad (1)$$

where γ is the mode Grüneisen parameter. $\alpha_\parallel$ and $\alpha_\perp$ are thermal expansion coefficients parallel and perpendicular to the c axis. Their temperature-dependent values can be found in [23] and [27]. $\omega(0)$ is the Raman frequency at 0 K. p_1 and p_2

Table 1. Fitting parameters for the temperature dependence of $E_{g(1)}$ Raman frequencies and linewidths.

$E_{g(1)}$ mode	$\omega(0)$ (cm^{-1})	p_1 (cm^{-1})	p_2 (cm^{-1})	Γ_o (cm^{-1})	Γ_o (300 K) (cm^{-1})	q_1 (cm^{-1})	q_2 (cm^{-1})
5.6 nm	140.0	1.813	−0.018	11.7	17.4	1.552	−0.032
8.6 nm	136.8	1.869	−0.016	6.1	12.3	1.477	−0.019
19.4 nm	135.9	1.809	−0.018	2.7	9.4	1.687	−0.022

are the anharmonic contributions to the Raman shift associated with zero-point motion. The first term of equation (1) is the thermal expansion contribution to the shift; the second and third terms are contributions from the anharmonic coupling to phonons of other branches, and they vary as T and T^2 at high temperatures (see figures 2 and 3). According to the simple Klemens model, the second term describes the coupling of an optical phonon to two low-energy phonons (a three-phonon process), the third term describes the coupling to three phonons (a four-phonon process), and $x = \hbar\omega(0)/2k_BT$, $y = \hbar\omega(0)/3k_BT$ [24, 28].

For the curve fitting, $\omega(0)$, p_1, and p_2 are taken as fitting parameters (three-parameter fitting). Figure 2 shows the three-parameter fittings to the experimental Raman peak data for the three nanocrystallites. The fitting parameters are listed in table 1. The Raman frequencies at 0 K, namely $\omega(0)$, for the 19.4, 8.6, and 5.6 nm nanocrystallites are 135.9, 136.8, and 140.0 cm^{-1}, respectively. The horizontal line in figure 2 acts as a guideline for better recognition of different contributions to the Raman shift. The contributions from the net thermal expansion, three-phonon processes and four-phonon processes are given as separate curves. At low temperatures (lower than ∼300 K) the main contribution to the hardening is the three-phonon process, as can be seen by the large ratios of $p_1/p_2 \sim$ 100–117. With increasing temperature, the hardening process slows down due to the opposite effects of the thermal expansion and four-phonon process contributions. It is noted that the extent of this hardening process decreases with decreasing nanocrystallite size or, in other words, the smaller crystallite has a lower blue-shift rate upon heating the nanocrystallite. The Grüneisen parameters of nanocrystalline and bulk TiO_2 are very similar to each other [4, 22]. In our calculations, therefore, we used the bulk value for all three samples, which was taken from [4].

The temperature dependence of the Raman linewidth can be written as [23]:

$$\Gamma(T) = (\Gamma(0) - q_1 - q_2) + q_1\left(1 + \frac{2}{e^x - 1}\right) + q_2\left(1 + \frac{3}{e^y - 1} + \frac{3}{(e^y - 1)^2}\right) \quad (2)$$

where, similarly to equation (1), the second and third terms correspond to three- and four-phonon processes, respectively. They vary as T and T^2 at high temperatures. q_1 and q_2 are the anharmonic contributions to the Raman linewidths associated with zero-point motion. $\Gamma(0)$ is the Raman linewidth at 0 K. Figure 3 shows the three-parameter fittings for the $E_{g(1)}$ linewidths of the three nanocrystallites. The fittings are excellent both at low and high temperatures. For the $E_{g(1)}$ mode, the main contribution comes from the three-phonon processes. This can be seen from the large ratio of q_1/q_2, which varies from 48 to 78. At high temperatures, the four-phonon processes become more important and counteract the effect from three-phonon processes. In all cases, the linewidth approaches a constant value as the temperature approaches zero; this is 2.7, 6.1, and 11.7 cm^{-1} for the 19.4, 8.6, and 5.6 nm nanocrystallites, respectively. On the other hand, it does not increase linearly with temperature above or below 300 K, as observed in single-crystal and nanocrystalline TiO_2 [2, 20]. Similarly to figure 2, both three- and four-phonon processes are needed to obtain good fitting, and also the linewidth for the smallest 5.6 nm nanocrystallite levels off more quickly than for the other two nanocrystallites.

At room temperature, the $E_{g(1)}$ peak frequency and linewidth for the bulk and the 19.4 nm nanoparticle are 144 and 7, and 141.8 and 9.4 cm^{-1}, respectively. Consider a possible instrument-induced uncertainty; the values for the 19.4 nm nanocrystallite are very near to those for a bulk crystal. Taking the 19.4 nm nanocrystallite as the reference sample, at room temperature the Raman peak frequencies and linewidths of the 8.6 and 5.6 nm nanocrystallites blue-shift by 2.0 and 4.3 cm^{-1}, and 2.9 and 8.0 cm^{-1}, respectively. Of these shifts, the contribution from the surface stress must be considered for nanodimensional particles. The surface stress is related to the surface free energy, which constitutes a significant part of the total free energy of nanoparticles. For a spherical nanocrystallite of diameter d, the pressure in the nanoparticle induced by the surface stress can be approximately estimated as $p = 4f/d$, where the surface stress for TiO_2 f is ∼1.5 J m^{-2} [4, 29]. This tensile stress will enlarge the lattice parameters of a and c. Our experimental results indeed showed increasing lattice parameters with decreasing nanoparticle size (0.3780, 0.3791, 0.3803 nm, and 0.9383, 0.9571, 0.9656 nm for a and c, respectively) for the 19.4, 8.6, and 5.6 nm nanocrystallites. The relative change in $\Delta a/\Delta c$ is 0.302, which is exactly the same as that of a theoretically predicted ratio of the linear compressibilities along the a and c directions [17]. This means that the tensile stress is of hydrostatic type in a spherical particle. Atomic force microscopy showed that the nanoparticles are indeed of near-spherical shape [30]. For the $E_{g(1)}$ mode, this tensile stress causes a frequency red-shift. Again, taking the 19.4 nm nanocrystallite as the reference sample, the red-shift of the $E_{g(1)}$ Raman peak induced by the surface stress is 1.0 and 2.0 cm^{-1}, respectively, for the 8.6 and 5.6 nm nanocrystallites. Here we use a frequency–pressure relationship of $d\nu/dp = 2.58$ cm^{-1} GPa^{-1} for the nano-anatase $E_{g(1)}$ mode [4].

For a nanodimensional crystallite, the phonon wavefunction is spatially restricted within an isolated nanoparticle. To describe this confinement, a confinement function must be superimposed on the Bloch-type wavefunction:

$$\varphi(\mathbf{q}, \mathbf{r}) = w(\mathbf{r}, d)\mu(\mathbf{q}, \mathbf{r})\exp(-i\mathbf{q}\cdot\mathbf{r}) \quad (3)$$

where $w(\mathbf{r}, d)$ is a confining function, $\mu(\mathbf{q}, \mathbf{r})$ is a function reflecting the crystalline periodicity, $\mathbf{q}$ is a wavevector, and $\mathbf{r}$ is a position vector in real space. This phonon confinement effect becomes noticeable only when the particle size d is smaller than ∼20 lattice parameters. For the case of TiO_2, this corresponds to a particle size of ∼7.6 nm in the a direction. Figure 4(a) shows the $E_{g(1)}$ Raman peaks for the three nano-size crystallites at room temperature. It can be seen that, for the 5.6 nm nanocrystallite, the $E_{g(1)}$ Raman spectrum has a considerable asymmetric broadening at the high-frequency side and a blue-shift compared to the 19.4 nm one. In the case of nanocrystals, according to the quantum uncertainty principle, the spatial restriction of the wavefunction results in a breakdown of the Raman selection rule of $\mathbf{q} \sim 0$. Phonons with a range of $\mathbf{q} \sim 0 - \pi/d$ near the Brillouin zone center will effectively take part in the first-order Raman scattering process. In the following discussions, we make the assumption that all phonons over the first Brillouin zone contribute to the Raman scattering [7, 21]. The wavefunction $\varphi(\mathbf{q}, \mathbf{r})$ is now a superposition of eigenfunctions, weighted by Fourier coefficients $C(0, \mathbf{q})$, of wavevectors in the whole Brillouin zone. The weight of off-center phonons increases as the crystal size decreases. For spherical nanocrystals and first-order Raman scattering, assuming a Gaussian confinement function for $w(\mathbf{r}, d)$, the Raman intensity $I(\omega)$ can be written as [7, 21, 31–33]:

$$I(\omega) = \int_{\mathrm{BZ}} \frac{|C(0, \mathbf{q})|^2 \, \mathrm{d}^3\mathbf{q}}{[\omega - \omega(\mathbf{q}, T)]^2 + (\Gamma_o(T)/2)^2}. \qquad (4)$$

Here, the integral is carried out in the whole first Brillouin zone (BZ). $\Gamma_o(T)$ includes the natural Raman linewidth of the bulk anatase, the anharmonic contribution given by equation (2), the contribution from the particle size distribution, and the instrumental and stress-induced broadening. $\omega(\mathbf{q}, T)$ is the phonon dispersion function. The Fourier coefficients $C(0, \mathbf{q})$, which we select as a strong phonon confinement function, can be expressed as [7, 21, 31–33]:

$$|C(0, \mathbf{q})|^2 = \exp\left(-\frac{q^2 d^2}{16\pi^2}\right). \qquad (5)$$

It can be seen from equation (5) that the weight of off-center phonons decreases as both the wavevector q and particle size d increase. In order to obtain the excellent calculations shown in figure 4, we found that a particle size distribution function $F(d)$ for each nominal nano-size sample must be included. In our calculations, the size distribution function was assumed to be of Gaussian type, which was deduced from the x-ray diffraction data. So the Raman intensity $I(\omega)$ can now be written as:

$$I(\omega) = \int_0^\infty F(d) I(\omega, d) \, \mathrm{d}d. \qquad (6)$$

The phonon dispersion induces an asymmetrical broadening and a Raman frequency shift [21, 31–33]. In principle, the phonon dispersion function in equation (4), $\omega(\mathbf{q}, T)$, should be an angular integral in the wavevector space of the first Brillouin zone along the Γ–X, Γ–N, and Γ–Z symmetry directions,

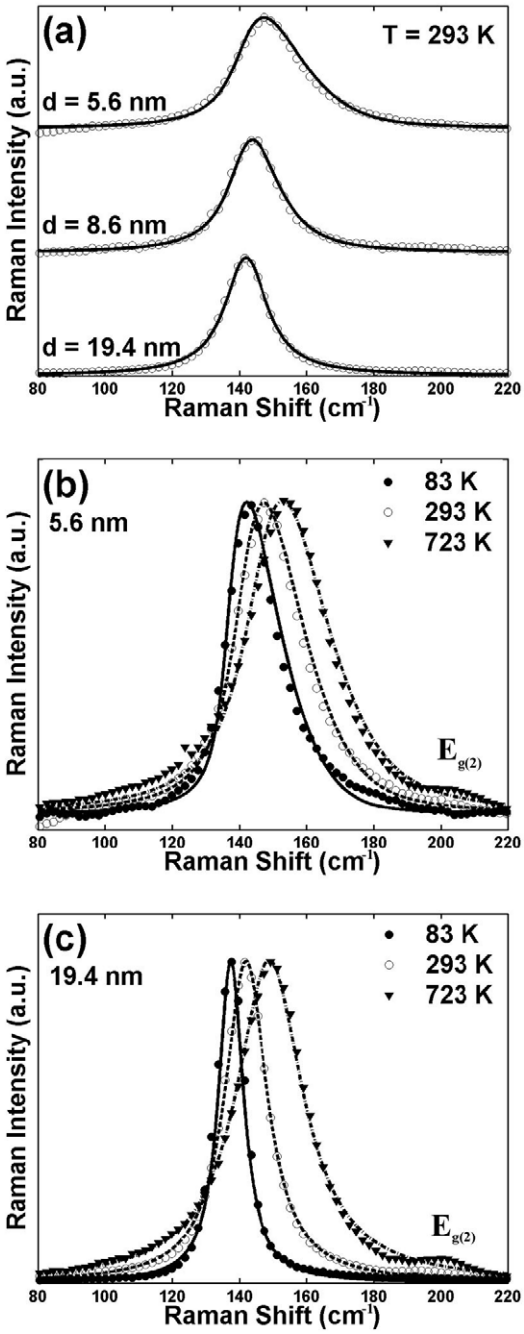

Figure 4. Experimental and calculated $E_{g(1)}$ Raman spectra: (a) Raman spectra for the three nanocrystallites recorded at room temperature and Raman spectra recorded at different temperatures for (b) 5.6 nm and (c) 19.4 nm nanocrystallites.

weighting each by the number of equivalent symmetry directions. The integrated contributions along the three directions have similar shape and peak position [3]. Therefore, in order to simplify the calculations, assuming a spherical Brillouin zone and an isotropic dispersion curve, the dispersion relationship for the $E_{g(1)}$ mode in anatase can be simplified as [7, 21, 33]:

$$\omega(\mathbf{q}, T) = \omega_o(T) + \Delta \times [1 - \cos(\mathbf{q} \times a)], \qquad (7)$$

where $\Delta = 20\ \mathrm{cm}^{-1}$, and $\omega_o(T)$ is the temperature-dependent Raman frequency for the bulk anatase. Using this simple

phonon dispersion function and equation (6), we get excellent Raman spectra calculations both at room temperature and low temperature for all the three nano-size crystallites, as shown in figure 4.

As discussed above, several factors can contribute to the changes in the Raman frequency and linewidth of the $E_{g(1)}$ mode in nanodimensional crystallites. These include phonon confinement, stress, anharmonicity, nano-size distribution, and the presence of possible oxygen vacancies [5]. The presence of possible oxygen vacancies would induce a hydrostatic compressive stress that leads to a blue-shift of the $E_{g(1)}$ mode. This effect counteracts that of the tensile stress induced by the surface stress. However, these two effects will be reflected collectively by the changed lattice parameters, as discussed above. For the Raman peak frequency of the 19.4 nm crystallite, the nano-size distribution leads to almost no peak shift and no linewidth change. For the 5.6 nm crystallite, calculations showed that the nano-size distribution leads to almost no peak shift and a linewidth increase of 1.4 cm^{-1}. As discussed above, at room temperature, taking the 19.4 nm nanocrystallite as the reference sample, the tensile stress-induced red-shifts are 1.0 and 2.0 cm^{-1}, respectively, for the 8.6 and 5.6 nm nanocrystallites. So the Raman peak shifts induced by the phonon confinement are 3.0 and 6.3 cm^{-1}, respectively, for these two nanocrystallites. Compared to the 19.4 nm crystallite, the linewidths increase by 2.9 and 8.0 cm^{-1}, respectively, for the 8.6 and 5.6 nm nanocrystallites. The stress-induced linewidth increases are only about 0.4 and 0.8 cm^{-1}, and the phonon confinement induced linewidth increases are 2.5 and 7.2 cm^{-1}, respectively, for these two nanocrystallites. The surface-stress-induced hydrostatic stress introduces a symmetric broadening. We can see that the phonon confinement has a comparative effect on both the linewidth broadening and the peak frequency.

The experimental data shown in figures 2 and 3 include all the effects discussed above that can induce a frequency shift and peak broadening. However, except for the anharmonic coupling, all the other effects, including the phonon confinement, surface stress, and instrumental broadening by the spectrometer, can be regarded as being temperature independent. The changes in both frequency and linewidth with increasing temperature can be regarded as being caused only by anharmonic coupling. The linewidth, $\Gamma_o(T)$, therefore can be written as an additive of the temperature-dependent $\Gamma(T)$ (equation (2)) and a temperature-independent Γ_o, i.e. $\Gamma_o(T) = \Gamma(T) + \Gamma_o$ [5, 34]. Γ_o can be obtained by extrapolating the experimental value of $\Gamma_o(T)$ to 0 K, which is listed in table 1. The phonon lifetime, $\tau_o(T)$, then can be written as an additive of the temperature-dependent $\tau(T)$ and a temperature-independent τ_o, i.e. $1/\tau_o(T) = 1/\tau(T) + 1/\tau_o$. From figures 2 and 3, it can be seen that for the 5.6 nm nanocrystallite, the extent of the temperature-dependent changes in both the Raman frequency and the linewidth are the smallest, while for the 19.4 nm nanocrystallite they are the largest. This shows that the phonon coupling is no faster in the smaller nanoparticles, and it has an even slower coupling rate in nanodimensional crystallites. Whether the phonon coupling is enhanced or not in a nanodimensional crystallite, the reported results are not consistent with each other. Both our results and a study of CeO_2 [5] considered not only three-phonon processes but also four-phonon processes, showing no enhanced phonon coupling in nanodimensional crystallites. However, the Raman studies of Si and TiO_2 showed an enhanced phonon coupling in nanoparticles [2, 34]. Both these works considered only three-phonon processes, and the experimental temperatures were only up to 300 K. Zhu *et al* obtained linear fittings to the experimental values of both the Raman frequency and the linewidth between 77 and 300 K [2]. The exact physical picture behind slower phonon coupling in a nanodimensional crystalline is not clear. In a large nanocrystallite (larger than ∼20 lattice parameters) or in a bulk-like crystal, the lattice vibration wave is described by a Bloch-type wavefunction. The two main phonon decay channels in a crystal are anharmonic phonon coupling and phonon scattering at defect centers, which include the crystal surface. In nanodimensional crystallites, the lattice vibration wave is described by equation (3), and it is reflected by the nearby surface boundaries and confined in a nanodimensional space. The phonon lifetime, τ, can be estimated via the energy–time uncertainty relation, $\Delta E/h = 1/\tau$, where ΔE is the Raman peak FWHM in units of cm^{-1} and $h = 5.3 \times 10^{-12}$ cm^{-1} s. At 0 K, the corresponding lifetimes are 2.0, 0.87, and 0.45×10^{-12} s, respectively, for the 19.4, 8.6, and 5.6 nm nanocrystallites. At very low temperatures, the phonons of the 5.6 nm crystal have a much shorter lifetime, and this is mainly decided by the confinement effect. With increasing temperature, the phonon density, which is given by the Bose–Einstein distribution function, $n(\omega, T) = [\exp(\hbar\omega/k_B T) - 1]^{-1}$, increases. The anharmonic-phonon-coupling-related decay increases. The anharmonic lattice vibration is evidenced itself by a crystal thermal volume expansion. As discussed above, for smaller nanocrystalline TiO_2, because of the surface stress, it is under relatively large tensile stress. It is more difficult to expand with increasing temperature compared to larger nanoparticles. The smaller nanoparticles, therefore, have slower anharmonic-phonon-coupling-related decay. It is interesting to note that at higher temperatures than the TiO_2 Debye temperature of 520 K, all three nanocrystallites have almost the same saturated linewidth of ∼20 cm^{-1}.

4. Concluding remarks

In conclusion, a detailed temperature-dependent Raman scattering study was carried out from 83 to 723 K for nanocrystalline anatase with nanocrystal sizes of 5.6, 8.6, and 19.4 nm. The lattice vibration fundamentals are essentially the same for all three nanocrystallites. Both the three- and four-phonon processes are needed to obtain excellent fitting, and the main contribution comes from the three-phonon processes. Compared to larger-grained TiO_2 crystal, the phonon coupling is slower in nanodimensional crystallites. At low temperatures, phonon confinement is responsible for the much shorter phonon lifetime. The anharmonic phonon coupling is responsible for the temperature-dependent increases in frequency and linewidth, while the effect from phonon confinement can be regarded as temperature independent.

References

[1] Blaji S, Djaoued Y and Robichaud J 2006 *J. Raman Sepctrosc.* **37** 1416
[2] Zhu K, Zhang M, Chen Q and Yin Z 2005 *Phys. Lett.* A **340** 220
[3] Scepanovic M J, Grujic-Brojcin M, Dohcevic-Mitrovic Z D and Popovic Z V 2007 *Appl. Phys.* A **86** 365
[4] Hearne G R, Zhao J, Dawe A M, Pischedda V, Maaza M, Nieuwoudt M K, Kibasomba P, Nemraoui O, Comins J D and Witcomb M J 2004 *Phys. Rev.* B **70** 134102
[5] Spanier J E, Robinson R D, Zhang F, Chan S W and Herman I P 2001 *Phys. Rev.* B **64** 245407
[6] Adu K W, Gutierrez H R, Kim U J and Eklund P C 2006 *Phys. Rev.* B **73** 155333
[7] Adu K W, Gutierrez H R, Kim U J, Sumanasekera G U and Eklund P C 2005 *Nano Lett.* **5** 409
[8] Verma P, Gupta L, Abbi S C and Jain K P 2000 *J. Appl. Phys.* **88** 4109
[9] Siefering K L and Griffin G L 1990 *J. Electrochem. Soc.* **137** 1206
[10] Logothetis E M and Kaiser W J 1983 *Sensors Actuators* **4** 333
[11] O'Regan B and Gräetzel M 1991 *Nature* **353** 737
[12] Asahi A, Taga Y, Mannstadt W and Freeman A J 2000 *Phys. Rev.* B **61** 7459
[13] Canginani G, Baldereschi A and Posternak M 2004 *Phys. Rev.* B **69** 121101
[14] Mikami M, Nakamura S, Kitao O and Arakawa H 2002 *Phys. Rev.* B **66** 155213
[15] Gonzalez R J, Zallen R and Berger H 1997 *Phys. Rev.* B **55** 7014
[16] Fahmi A, Minot C, Silvi B and Causa M 1993 *Phys. Rev.* B **47** 11717
[17] Calatayud M, Mori-Sanchez P, Beltran A, Pendas A M, Francisco E, Andres J and Recio J M 2001 *Phys. Rev.* B **64** 184113
[18] Du Y L, Deng Y and Zhang M S 2006 *J. Phys. Chem. Solids* **67** 2405
[19] Ohsaka T, Izumi F and Fujiki Y 1978 *J. Raman Spectrosc.* **7** 321
[20] Ohsaka T 1980 *J. Phys. Soc. Japan* **48** 1661
[21] Bersani D, Lottici P P and Ding X 1998 *Appl. Phys. Lett.* **72** 73
[22] Swamy V, Kuznetsov A, Dubrovinsky L S, Caruso R A, Shchukin D G and Muddle B C 2005 *Phys. Rev.* B **71** 184302
[23] Wang D, Chen B and Zhao J 2007 *J. Appl. Phys.* **101** 113501
[24] Balkanski M, Wallis R F and Haro E 1983 *Phys. Rev.* B **28** 1928
[25] Li W S, Shen Z X, Feng Z C and Chua S J 2000 *J. Appl. Phys.* **87** 3332
[26] Alim K A, Fonoberov V A and Balandin A A 2005 *Appl. Phys. Lett.* **86** 053103
[27] Krishna Rao K V, Nagender Naidu S V and Iyengar L 1970 *J. Am. Ceram. Soc.* **53** 124
[28] Klemens P G 1966 *Phys. Rev.* **148** 845
[29] Zhang H and Banfield J F 1998 *J. Mater. Chem.* **8** 2073
[30] Wang D, Zhang X, Wu K and Xu S 2006 *Chem. Lett.* **35** 884
[31] Richter H, Wang Z P and Ley L 1981 *Solid State Commun.* **39** 625
[32] Campbell I H and Fauchet P M 1986 *Solid State Commun.* **58** 739
[33] Zhang W F, He Y L, Zhang M S, Yin Z and Chen Q 2000 *J. Phys. D: Appl. Phys.* **33** 912
[34] Mishra P and Jain K P 2000 *Phys. Rev.* B **62** 14790